Facile synthesis of ZnS quantum dots at room temperature for ultra-violet photodetector applications

Rujie Li[a,b,c], Libin Tang[a,b,c*], Qing Zhao[a**], Kar Seng Teng[d***], Shu Ping Lau[e]

[a] *School of Physics, Beijing Institute of Technology, Beijing 100081, China*
[b] *Kunming Institute of Physics, Kunming 650223, Yunnan Province, China*
[c] *Yunnan Key Laboratory of Advanced Photoelectric Materials & Devices, Yunnan Province, China*
[d] *College of Engineering, Swansea University, Bay Campus, Fabian Way, Swansea SA1 8EN, United Kingdom*
[e] *Department of Applied Physics, The Hong Kong Polytechnic University, Hung Hom, Kowloon, Hong Kong*

Abstract

Zinc sulfide (ZnS) quantum dots (QDs) were synthesized using a facile, low-cost and environmentally friendly method at room temperature and ambient pressure. The structural, optical and electrical properties of the as-prepared ZnS QDs were investigated. The monodispersed crystalline ZnS QDs with an average size of 3.8 nm has been prepared, an absorption peak at 292 nm in the ultra-violet (UV) range was observed. The maximum responsivity (R) and detectivity (D^*) of the ZnS QDs based photodetector under 365 nm UV light illumination were 5.8 A W^{-1} and 1.97×10^{13} Jones, respectively, which shows important potential application in UV detection.

1. Introduction

Quasi-zero-dimensional semiconductor quantum dots (QDs) exhibit many unique and excellent physical, electronic and optical properties that offer a wide range of applications with new functionalities [1,2]. Zinc sulfide (ZnS), which is a II-VI binary compound with direct wide bandgap, is an important metal chalcogenide material. Zero-dimensional ZnS QDs are of particular interest as both electrons and holes are confined in all three dimensions leading to an increase in its bandgap energy and exciton energy. Thus, its optical bandwidth can be altered by the size of the QDs due to quantum size effect. Moreover, ZnS QDs exhibit non-toxicity and good chemical stability as compared with other semiconductor QDs. Therefore, ZnS QDs are suitable for application in light-emitting diodes (LEDs), electroluminescent devices, optoelectronic devices and photocatalysis for water treatment etc [3-6].

Although ZnS QDs have found many potential applications, most current methods used in the synthesis of the material are unsuitable for large-scale low-cost production. There are various methods of synthesizing QDs, such as liquid-phase exfoliation (LPE) [7], solution thermal synthesis[8], hot injection[9,10], and wet chemistry methods[11]. However, these methods require expensive equipment, highly concentrated acid or high temperature and pressure conditions, which can limit scale up production. Though the use of microwave irradiation offers a quick and easy method of synthesizing QDs in a few minutes, the uncontrollable reaction can limit its utility[12].

Another method of synthesizing ZnS QDs is by colloidal method, which is a wet chemical method based on non-covalent routes using surfactants and polyelectrolytes [13]. Such low-temperature, low-cost, large-scale solution-based synthesis method is highly favorable for volume production. Furthermore, colloidal semiconductor QDs can potentially combine with other nanomaterials for high performance device applications [14]. Such colloidal QDs are of significant scientific and technological interests as they can be used to develop novel devices with new applications.

In this paper, a facile and efficient method to synthesize ZnS QDs has been studied. It does not require high temperature and pressure. Compared with traditional microemulsion method, the wet chemical liquid phase synthesis method possessed milder conditions, convenient process and more economical precursors and equipments. The growth technique can be extended to other semiconductor/sulfide systems. The physical, chemical and optical properties of the as-prepared ZnS QDs were investigated using multiple characterization techniques. This work demonstrated the synthesis of small and homogeneous ZnS QDs, which showed good dispersion and stability in solvent. Photodetector based on the ZnS QDs was also fabricated. The device exhibited excellent detectivity under ultra-violet (UV) illumination, which suggests ZnS QDs have great potential for application in UV photodetector.

Corresponding authors.
E-mail addresses: * Corresponding author: scitang@163.com (L.B. Tang), ** Corresponding author: qzhaoyuping@bit.edu.cn (Q. Zhao),
***Corresponding author: k.s.teng@swansea.ac.uk (K.S. Teng)

2. Experimental

2.1. Chemicals and reagent

$(CH_3COOH)_2Zn{\cdot}H_2O$, $Na_2S{\cdot}9H_2O$ (98.0%) and $C_{12}H_{25}NaO_3S$ (SDS 98.0%) were purchased from Tianjin Fengchuan Chemical Reagent Co. Ltd. (Tianjin,China). Ethylene glycol was purchased from Chengdu Kelong Chemical Co. Ltd. (Sichuan, China). Dialysis bag (USA spectrum lab's regenerated cellulose membrane, Mw = 100) was purchased from Shanghai Yibai Economic and Trade Co. Ltd. All metal salts were dissolved in deionized water. All chemicals were of analytical grade and used without further purification.

2.2. Preparation of ZnS QDs

Sulfur and zinc precursors, such Na2S (0.1 mol/L) and $(CH_3COOH)_2$ Zn (0.1 mol/L) respectively, were first dissolved in deionized water. Then 0.08 mol/L (critical micelle concentration, CMC) of $C_{12}H_{25}NaO_3S$ (sodium dodecyl sulfate, SDS) as surfactant were added to both Na_2S and $(CH3COOH)_2Zn$ solutions (volume ratio of 1:1). Subsequently, the mixed Na_2S solution was slowly dripped into the mixed $(CH_3COOH)_2$ Zn solution under constant stirring for 10 min at room temperature (RT). A milky white appearance of the reacted mixture was an indication of ZnS formation. The reacted mixture was then centrifuged at 3000 rpm for 5 min to remove any oversized and unwanted particles. This process was repeated three times. Finally, the mixture was dialyzed for one day to obtain pure ZnS QDs. The as-prepared ZnS QDs were collected and preserved in ethylene glycol (as dispersant).

2.3. Characterization techniques

As-prepared ZnS QDs were characterized and studied using a variety of analytical techniques. The shape and size of the QDs were characterized using Transmission Electron Microscope (TEM, JEM-2100 electron microscope operating at 200 kV). Surface morphology was studied by atomic force microscopy (AFM, SPA-400). The crystallinity of the QDs was analyzed by X-ray diffractometer (XRD, Rigaku D/Max-RA) with Cu Ka radiation. Surface functional groups at the ZnS QDs were investigated using x-ray photoelectron spectroscopy (XPS, PHI Versa Probe II) using Al Ka radiation. UV-visible spectrophotometer (SHIMADZU, UV-3600) and fluorescence spectrophotometer (Hitachi F-4500) were used to study the optical properties of the QDs. The fluorescence effect was analyzed using a camera-obscura ultraviolet analyzer (ZF-7N). Measurement of current density–voltage (*J–V*) characteristic of the ZnS QDs based photodetector was performed using semiconductor device analyzer (Keysight B1500A). LEICA optical microscope (DM 2700M) was used to capture the images of the interdigital electrodes.

3. Results and discussion

3.1. Growth mechanism of ZnS QDs

ZnS QDs were synthesized at atmospheric pressure and room temperature using a low-cost, facile preparation method (Scheme 1). The method was developed from a previously reported synthesis technique based on chemical bath deposition of ZnS QDs [15].The SDS, which was used as surfactant, served three main purposes. First purpose was to control the growth rate of QDs by controlling the rate of nucleation, hence improving the size uniformity of the QDs. Second purpose of SDS was to act as colloidal stabilizer by attaching its sulfonic group to the QDs. It stabilized surface of the QDs would result in monodispersed QDs. Finally, it was also used to passivate the QDs, which would lead to electrostatic and steric stability of the QDs.

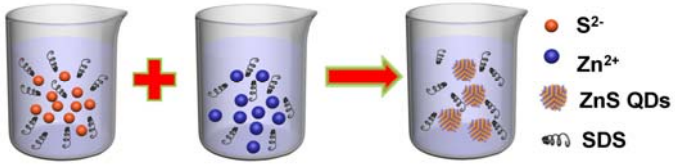

Scheme 1. Schematic representation of the synthesis of ZnS QDs at atmospheric pressure and room temperature conditions.

3.2 Characterization of ZnS QDs

TEM image shown in Fig. 1a revealed the spherical and well dispersed as-prepared ZnS QDs. Fig. 1d shows the size distribution of the QDs, which can be fitted with a Gaussian curve, and it ranged from 2 to 6 nm with an average size of 3.8 nm. The full-width-at-half-maximum (FWHM) of the Gaussian curve was 2.1 nm. Fig. 1b and 1c are HRTEM images of the ZnS QDs showing the lattice fringes for d = 0.271 and 0.313 nm, corresponding to the square crystal system of (220) and (111) lattice planes, respectively [16]. The clear and bright lattice fringes demonstrated good crystallinity of the QDs. An inter-planar crystal spacing of 0.320 nm was measured from the line profile, shown in Fig. 1e, taken along the red line at the lattice planes in Fig. 1c. Fig. 1f shows the morphology of the ZnS QDs obtained using AFM. Height measurements (Fig. 1g) were performed on randomly selected QDs, which were indicated as 'A','B' and 'C' in Fig. 1f, the measured heights were 4.5, 3.3 and 4.1 nm, respectively. An average height of 4.0 nm from the AFM measurements is very close to that obtained from the TEM image. Fig. 1h shows the XRD pattern of the ZnS QDs. The peaks at 2θ = 28.50, 47.48 and 56.31 corresponded to the lattice planes (111), (220) and (311), respectively [17]. This suggests that the space group of ZnS QDs is F-43m and belongs to cubic crystal system. The zinc ions are located at the apex corner of the cell, as shown in inset of Fig. 1h. This is consistent with previously reported work [18].

The chemical composition and bonding states at the ZnS QDs were investigated using XPS. Fig .2a shows the full XPS spectrum, consisting of S2p3/2, S2p1/2, Zn2p3/2 and Zn2p1/2 at 161.3, 227.1, 1023.9 and 1048.3 eV, respectively [19].The deconvoluted peaks revealed the bonding states of S2p (Zn-S and C-S) and Zn2p (Zn-S and Zn-O). Core level peaks of S2p and Zn2p are shown in Fig. 2b and 2c, respectively. In addition to the main elements of ZnS QDs, C and O peaks were also observable. The presence of these peaks could due to the C and O functional groups introduced by the surfactant. XPS results of ZnS QDs showed the existence of Zn, S along with little amount of C and O, which confirms the presence of surfactant functional groups at the surface of ZnS QDs. This observation can be explained as follows: ZnS QDs synthesized in the present work has been passivated by SDS, which not only control the growth rate of nucleation, but also ensure stability of the monodispersed QDs.

3.3 Optical properties of the ZnS QDs

The optical properties of the as-prepared ZnS QDs were investigated for application in optoelectronics. An absorption peak at 292 nm in the ultraviolet range was evident in ultraviolet-visible (UV-vis) absorption spectrum shown in Fig. 2d. Compared with ZnS bulk materials, the absorption peak position indicates blue shift due to the quantum size effect of the QDs. Since ZnS is a direct bandgap material, its optical bandgap energy Eg can be expressed using the Tauc plot. From the plot of $(ahv)^2$ vs. hv (as shown in the inset of Fig .2d), the estimated bandgap energy of the ZnS QDs was 4.3 eV.

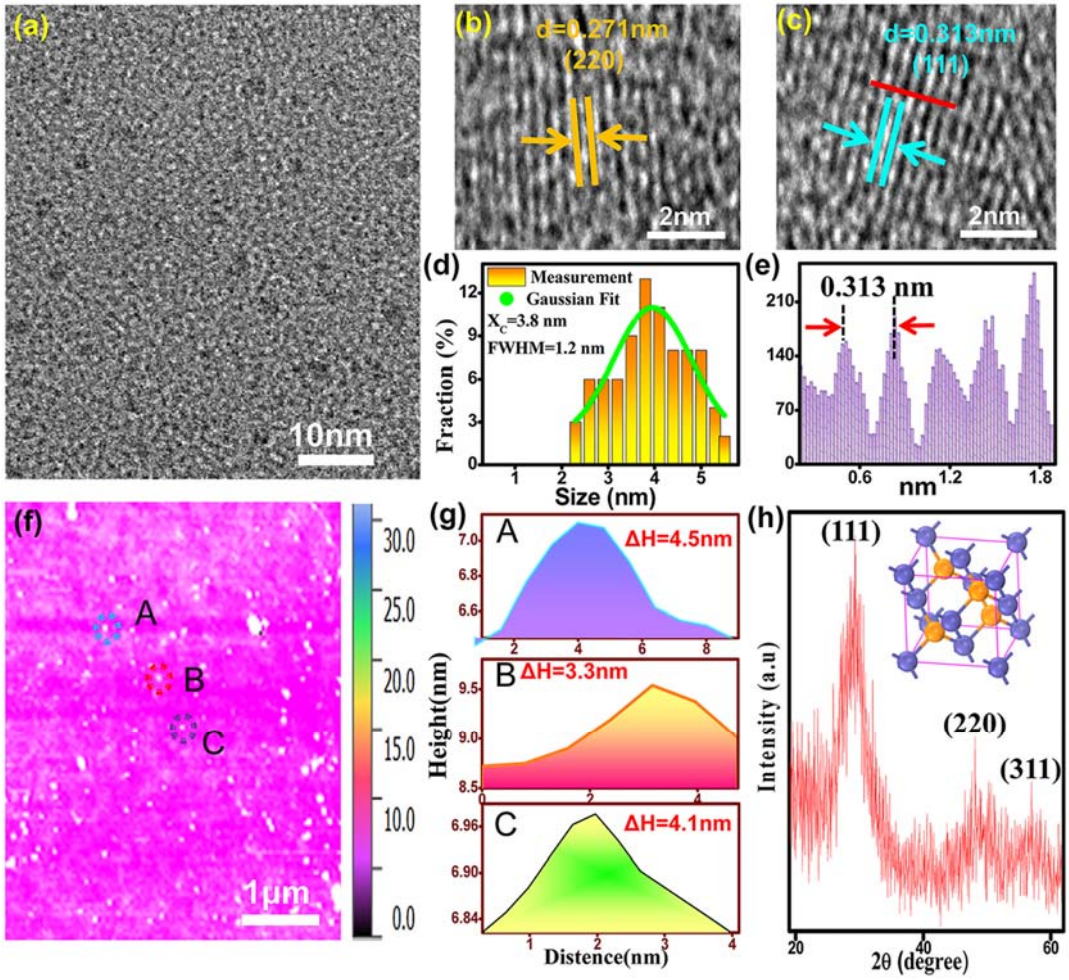

Fig. 1. (a) TEM image of ZnS QDs. (b-c) HRTEM images of the ZnS QDs showing lattice fringe spacing of 0.271 and 0.313 nm, respectively. (d) Histogram showing size distribution of as-prepared ZnS QDs (e) Line profile of the diffraction fringes in (c). (f) AFM image of the ZnS QDs. (g) Height measurements of randomly selected QDs labeled as 'A', 'B' and 'C' in (f). (h) XRD spectrum of the as-prepared ZnS QDs (inset: schematic of the crystal cell structure).

Photoluminescence (PL) emission spectra of ZnS QDs at room temperature are shown in Fig. 2e. The QDs solution was excited at wavelength from 225 to 325 nm and the PL spectra showed fluorescence emission spectra centered at 420 nm, no obvious excitation-dependent emission has been observed. As shown in inset of Fig. 2e, the QDs solution (on the left) appeared pale white under visible light and exhibited strong blue emission (on the right) under 365 nm ultraviolet illumination, hence demonstrating the fluorescent nature of the as-prepared ZnS QDs. The PLE spectra at a wavelength range of 400 to 480 nm on the ZnS QDs is shown in Fig. 2f. Broad PLE peaks can be observed at ~ λ=314 nm with different emission energies (λ_{Em}). Fig. 2f. also shows that PLE peak just has a 4 nm shift as increasing receiving wavelength from 400 nm to 480 nm, indicating a rather weak λ_{Em} dependent PLE peak. However, the mechanism of strong fluorescence is debatable. Previous studies suggested that the blue fluorescence was due to the bandgap as a results of localization of electron-hole pairs in nano-sized sp2 hybridized domains [20]. However, in this case, the presence of hydroxyl moieties from SDS could play a major role in the blue fluorescence emission observed at the as-prepared ZnS QDs solution.

3.4 Device of the ZnS QDs fabrication and characterization

As the ZnS QDs exhibited excellent UV absorption properties, UV photodetector based on the ZnS QDs was fabricated and studied. The fabrication process of the photodetector is illustrated in Fig. 3a. Quartz substrate was washed with acetone, alcohol and distilled water for 10 min at each step in an ultrasonic bath. Next, the substrate was heated at 80 °C for 15 min. Then, a 400 nm thick Au/Cr film at a ratio of 4:1 was deposited on the substrate. Cr was used to improve the adhesion of the Au film on the substrate. Interdigital electrodes with finger length of 120 μm and width and spacing of 10 μm was fabricated using lithography technique[21]. The QDs solution was then drop-casted on the interdigital electrodes and dried at 50 °C on a hot plate in air to form a layer of ZnS QDs with an estimated thickness of 400nm. The inset of Fig. 3d shows an optical image of the interdigital electrodes with deposited ZnS QDs. A homogeneous white QDs film as a photosensitive layer can be observed from the image.

The current density against voltage (*J-V*) curves of the ZnS photodetector measured in dark condition and under irradiation of 365 nm UV light with power densities of 0.01, 0.06, 0.16, 0.40 and 0.47 mW cm^{-2} are shown in Fig. 3b. The current increased exponentially with applied potential under both forward and reverse biased conditions, hence demonstrating the presence of a Schottky barrier without annealing. Unlike the rectifying characteristic, the current generated by the reverse bias voltage is mainly due to the symmetrical interdigital electrodes of the device. Fig. 3c shows the log(*J-V*) curve, which revealed a greater light current as compared to the dark current. Furthermore, The performance of the photodetector was stable as the *J-V* curve remained the same for repeated measurements. As demonstrated, the ZnS QDs is highly suitable for use as UV detector due

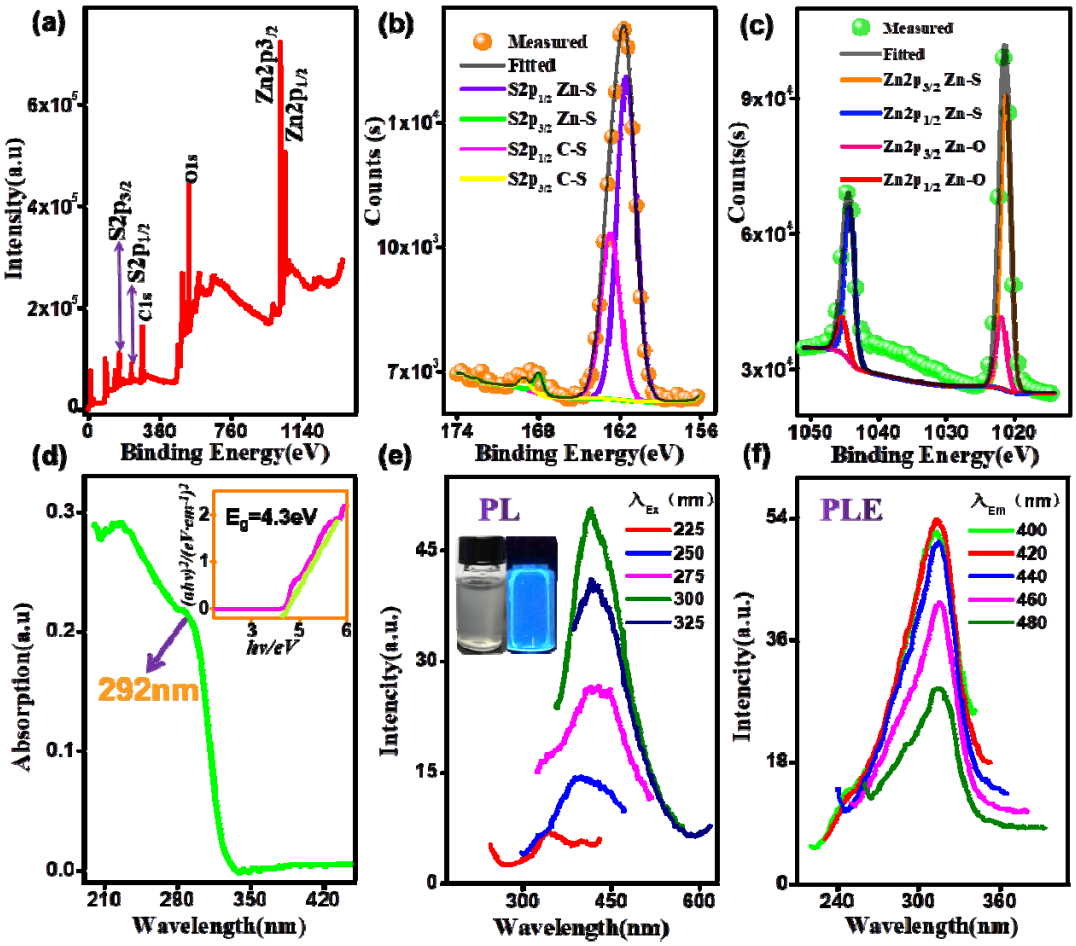

Fig. 2. (a) XPS full spectrum of ZnS QDs film. (b -c) XPS spectra of S2p and Zn2p core levels, respectively. (d) UV-Vis absorption spectrum of ZnS QDs aqueous solution (inset: Tauc plot for estimating bandgap energy of ZnS QDs) (e) PL emission spectra (inset: optical image under visible and 365 nm light source) and (f) PLE spectra of the ZnS QDs aqueous solution.

to its wide bandgap and high electron mobility (600 $cm^2V^{-1}s^{-1}$) [22]. Responsivity (R) and detectivity (D*) of the ZnS QDs photodetector can be obtained using the following equations [23]:

$$R = J_{ph} / P_{opt} \tag{1}$$

$$D^* = \frac{R}{\sqrt{2q / J_d}} \tag{2}$$

where J_{ph} is photocurrent density, P_{opt} is photo power density, q is absolute electron charge and J_d is dark current density.

This result, the value of R is increasing with decreasing of the reverse bias voltage, the forward voltage is just the opposite, *R* is symmetrical at zero. From Fig. 3d, the maximum value of *R* is 5.83 A W^{-1}, which is significantly larger than graphene and many other two-dimensional nanomaterial based photodetectors[24-26]. Fig. 3e shows a plot of *D** against voltage. It showed that the *D** stabilized at around 10^{11} Jones (1 Jones = 1cm·$Hz^{1/2}W^{-1}$) and the *D** peak reached 10^{13} Jones. The energy band diagram of the ZnS photodetector is shown in the inset of Fig. 3e and is used to illustrate the photoelectric detection mechanism of the photodetector. When UV light irradiates on the device, UV photons are absorbed by the photosensitive ZnS QDs. Electrons are excited from the valence band (VB) to the conduction band(CB)[27], forming photogenerated electrons and holes (excitons). Under the biased electric field, these excitons are separated and collected by the electrodes.

4. Conclusion

In this work, ZnS QDs with good crystallinity were successfully prepared using a low-cost, facile, green and effective method under ambient pressure and room temperature conditions. The physical, chemical and optical properties of the ZnS QDs have been studied using a variety of characterization techniques. The ZnS QDs has an average size of 3.8 nm. They showed excellent homogeneity and monodispersity due to the surfactant functional moieties at its surface. A photodetector based on ZnS QDs as the sole photoactive material was fabricated. It exhibited a high detectivity of 1.9×10^{13} Jones at room temperature under 365 nm UV light illumination without preamplifier.

Declaration of Competing Interest

The authors declare that they have no known competing financial interests or personal relationships that could have appeared to influ- ence the work reported in this paper.

Acknowledgments

This work was supported by National Natural Science Foundation of China (No. 61106098), Equipment Pre-research Fund under the Equipment Development Department (EDD) of China's Central Military Commission (CMC) (No.1422030209), the Innovation Team Program of NORINCO Group (No.2017CX024), and Yunnan Key Laboratory of Advanced Photoelectric Materials & Devices.

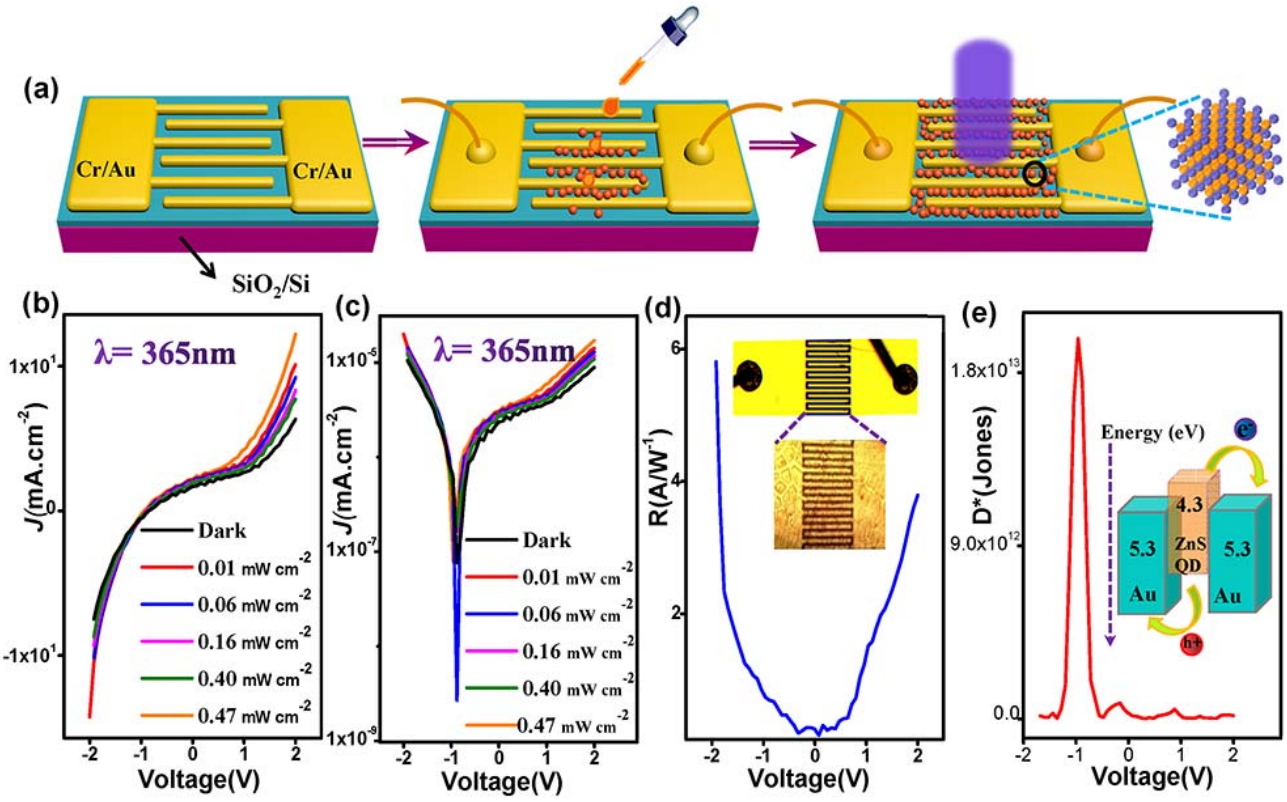

Fig. 3. (a) Schematic diagrams illustrating the fabrication process of the ZnS QDs photodetector. (b-c) Plots of *J–V* and *log(J)–V* curves of the photodetector in the dark and under 365 nm UV light illumination at different power densities, respectively. (d-e) Plots of *R-V* and *D*-V* curves of the ZnS photodetector (inset: (d) optical image of the interdigital electrodes and (e) energy band diagram of the photodetector), respectively.

References

1. C. R. Kagan, E. Lifshitz, E. H. Sargent, D. V. Talapin, Building devices from colloidal quantum dots, Mater. Sci. 353 (2016) 885.

2. J.S.J. Prakash, G. Vinitha, M. Ramachandran, K. Rajamanickam, Analysis on non-linear optical properties of Cd(Zn)Se quantum dots synthesized using three different stabilizing agents, Opt. Mater. 72 (2017) 821-827.

3. X. Dai, Z. Zhang, Y. Jin, Y. Niu, H. Cao, X. Liang, L. Chen, J. Wang, X. Peng, Solution-processed, high-performance light-emitting diodes based on quantum dots, Nature 515 (2014) 96.

4. N. Demir, I. Oner, C. Varlikli, C. Ozsoy, C. Zafer, Efficiency enhancement in a single emission layer yellow organic light emitting device: contribution of CIS/ ZnS quantum dot, Thin Solid Films 589 (2015) 153.

5. L.K. Sarponga, M. Bredola, M. Schönhoffb, et al., One-pot synthesis of carbon nanotube/zinc sulfide hetero structures: Characterization and effect of electrostatic interaction on the optical properties, Opt. Mater. 86 (2018) 398-407.

6. S. Feng, J. Zhao, Z. Zhu, The manufacture of carbon nanotubes decorated with ZnS to enhance the ZnS photocatalytic activity, N. Carbon Mater. 23 (2008) 228-234.

7. A. S. Ethiraj, D. Rhen, D. H. Lee, D. J. Kang, S. K. Kulkarni, Investigation of thioglycerol stabilized ZnS quantum dots in electroluminescent device performance, AIP Conference Proceedings (2016) 1728, 020554.

8. L. Sang, M. Liao, M. Sumiya, A comprehensive review of semiconductor ultraviolet photodetectors: From thin film to one-dimensional nanostructures, Sensors 13 (2013) 10482–10518.

9. M. M. Fan et al., High-performance solar-blind ultraviolet photodetector based on mixed-phase ZnMgO thin film, Appl. Phys. Lett. 105 (2014) 011117.

10.J.-H. Choi et al., Exploiting the colloidal nanocrystal library to construct electronic devices. Science 352 (2016) 205-208.

11.Y. Li, L.B. Tang, R.J. Li, et al., SnS_2 quantum dots: Facile synthesis, properties, and applications in ultraviolet photodetector Chin. Phys. B Vol. 28, No. 3 (2019) 037801.

12.D. Bano, V. Kumar, V.K. Singh, S.H. Hasan, Green synthesis of fluorescent carbon quantum dots for the detection of mercury (ii) and glutathione, New J. Chem. 42 (2018) 5814-5821.

13.Yasuhiro Shirasaki, Geoffrey J. Supran, Moungi G. et al., Emergence of colloidal quantum-dot light-emitting technologies, Nat. Photonics 7 (2013) 13-23.

14.J. Yang, M. K. Choi, D.-H. Kim, T. Hyeon, Designed assembly and integration of colloidalnanocrystals for device applications. Adv. Mater. 28, (2016) 1176-1207.

15.J.H.K.G.L. Agawane, S.W. Shin, M.S. Kim, M.P. Suryawanshi, K.V. Gurav, A.V. Moholkar, J.Y. Lee, J.H. Yun, P.S. Patil, Green route fast synthesis and characterization of chemical bath deposited nanocrystalline ZnS buffer layers, Curr. Appl. Phys. 13 (2013) 850-56.

16.U. Jabeen, T. Adhikari, Syed M. Shah, Dinesh Pathak, J.-M. Nunzi, Synthesis, characterization and photovoltaic performance of Mn-doped ZnS quantum dots- P3HT hybrid bulk heterojunction solar cells, Opti.l Mater. 73 (2017) 754-762.

17.H.R. Rajabi, M. Farsi, Effect of transition metal ion doping on the photocatalytic activity of ZnS quantum dots: synthesis, characterization, and application for dye decolorization, J. Mol. Catal. A Chem. 399 (2015) 53–61.

18.Y.N. Zhang, D. Jiang, Z. He, Y.W. YU, H.B. Zhang Z.H. Jiang,

Hydrothermal Synthesis of PEG-capped ZnS:Mn^{2+} Quantum Dots Nanocomposites, Chem. Res. Chin. Univ., 30(1), (2014) 176-180.

19.H. Labiadh, B. Sellami, A. Khazri, et al., Optical properties and toxicity of undoped and Mn-doped ZnS semiconductor nanoparticles synthesized through the aqueous route, Opt. Mater. 64 (2017) 179-186.

20.C. Murray, C. Kagan, M. G. Bawendi, Synthesis and characterization of monodisperse nanocrystals and closepacked nanocrystal assemblies. Annu. Rev. Mater. Sci. 30, (2000) 545-610.

21.Tang L, Ji R, Li X, Bai G, Liu CP, Hao J, Lin J, Deep Ultraviolet to Near-Infrared Emission and Photoresponse in Layered N-Doped Graphene Quantum Dots. ACS Nano 8 (2014) 6312-6320.

22.W. Martienssen, H. Warlimont, Springer Handbook of Condensed Matter and Materials Data, first ed., Springer, New York, 2005, 671.

23.S. Jindal, S.M. Giripunje, Potential effect of $CuInS_2$/ZnS core-shell quantum dots on P3HT/PEDOT: PSS heterostructure based solar cell, Optics and Laser Technology 103 (2018) 212-218.

24.W. Huang, L. Gan, H. Yang, N. Zhou, R. Wang, W. Wu, H. Li, Y. Ma, H. Zeng, T. Zhai, Controlled Synthesis of Ultrathin 2D β-In_2S_3 with Broadband Photoresponse by Chemical Vapor Deposition, Adv Funct Mater (2017) 27(36).

25.Tabitha A. Amollo, Genene T. Mola, Vincent O. Nyamori, Polymer solar cells with reduced graphene oxide–germanium quantum dots nanocomposite in the hole transport layer, J Mater. Sci.: Materials in Electronics (2018) 29: 7820-7831.

26.Y.H. Cai, L.B. Tang, J.Z. Xiang, R.B. Ji, J. Zhao, J. Yuan, et al, Exceptional ultraviolet photovoltaic response of 2, 9-dimethyl-4, 7-diphenyl-1, 10-phenanthroline based detector, Appl. Phy. Hysics (2015) 118, 124503.

27.W.J. Kuang, X. Liu, Q. Li, Y.Z. Liu, J. Su, H. Tolner, Solution-Processed Solar-Blind Ultraviolet Photodetectors Based on ZnS Quantum Dots, IEEE Photo. Tech. Lett., (2018) 30 1384-1387.